Delft University of Technology
Department of Radiation Science & Technology
section Reactor Physics and Nuclear Materials

Bachelor Final Project Applied Physics

An experimental analysis of two-phased flow patterns inside a microchannel

Author:
Tymen Nanninga (4315421)

Supervisors:
Martin Rohde
Zheng Liu

February 14, 2018

Abstract

The goal of this research was to provide an experimental analysis of flow patterns inside a double y-junction microchannel. Various flow patterns were observed, ranging from droplet formation to no leakage parallel flow (NLPF).

Viscous forces are the dominant factor in determining flow patterns in the IMT chip, if the interface stabilizes itself near the width $w^* = \frac{1}{2}w$, for Reynolds numbers in the order of $10^0 < Re < 10^1$ and for capillary numbers in the order of $10^{-4} < Ca < 10^{-3}$. The stability of parallel flow is impacted negatively by the surface tension force and the inertial forces present in the system.

The viscous forces are dependant on the velocity ratios and the viscosity ratios of the liquid phases. For high relative viscous forces, droplet flow patterns will be observed, while for relative viscous forces equaling unity, different parallel flow patterns are observed.

NLPF was established with the IMT chip. However, due to instability of the flow, caused by the surface tension and the inertial forces, but possibly also by the perturbation of the pumps, the NLPF only stabilized for short periods.

In the case of the Micronit chip, it was observed that the wettability of the channel was a major destabilizing factor for the flow patterns observed. NLPF was not found in this chip, due to inevitable parallel aqueous leakage into the organic phase outlet. By selectively coating the chip with a hydrophobic layer, parallel flow was stabilized. This resulted in a large, stable NLPF relative viscous forces range. A higher total viscous force at the outlet of the channel seems preferable for stability of parallel flow. This renders small variable changes negligible.

Contents

1 Introduction

The use of micro-scale devices in fluid dynamics has shown great potential in this decade. It has found applications in several chemical processes, including nitration[1], emulsification [2], and extraction[3]. Micro-scale lab-on-a-chip devices offers unique advantages, such as a high specific inter-facial area, improving mass and heat transfer[4][5], and extremely laminar conditions, due to the low flow rates and small chip dimensions.

The Reactor Physics and Nuclear Materials department of the Reactor Institute Delft is currently looking into a possible application of micro-scale fluidic systems. It tries to extract a radioactive isotope, Molybdenum-99, from an aqueous phase which also contains other radioactive elements. Currently, a decay product of molybdenum-99 is used in the medical field. Specifically, technetium-99m, the decay product, is used as the main radioactive tracer in radioactive imaging[6].

The extraction is attempted through a liquid-liquid two phase flow, inside a double y-junction micro-channel. Typically, y-junction micro-channels are used in micro-scale extraction devices, as rapid stabilization of the interface can be achieved this way[7]. It has been shown that two-phased parallel flow is possible inside a micro-channel [8]. This process was integrated into the Molybdenum-99 extraction so that pure mass transfer could be achieved, without any emulsification after flow separation in the channel. It was vital that a non-polluted solute of Molybdenum-99 was acquired. The use of a micro-scale device also allowed for optimal diffusion of the Molybdenum-99, due to the extremely low flow rates.

Before extraction experiments can be initiated, flow patterns must be analyzed. This study's goal is provide an experimental analysis of the governing factors in the formation of flow patterns inside a double y-junction micro-channel, such as absolute and relative flow rates and surface tension and to achieve non-leakage parallel flow, through flow pattern analysis.

2 Theory

2.1 Navier-Stokes equations

The Navier-Stokes equations describe the motion of Newtonian fluids. They relate to Newton's second law of physics. Where Newton's second law describes the motion of a mass M, the Navier-Stokes equations describe a volume S with density ρ, thus also working with force densities. Here, the equations are given for a single fluid[10].

$$\rho \frac{\partial \mathbf{v}(r(t),t)}{\partial t} = \sum_j f_j \tag{2.1}$$

Where $\sum_j f_j$ are the all the force densities acting on the system. Since the velocity v as well as its position r are both dependant on time, taking the total time derivative of $\mathbf{v}(r(t),t)$ results in

$$\frac{\partial \mathbf{v}(r(t),t)}{\partial t} = \frac{\partial \mathbf{v}(r(t),t)}{\partial t} + \frac{\partial \mathbf{r}(t)}{\partial t} \cdot \frac{\mathbf{v}(r(t),t)}{\partial_i} \tag{2.2}$$

Where the ∂_i represents the spacial derivative for three dimensions, which produces a nabla operator term $\bigtriangledown$

$$\rho \frac{\partial \mathbf{v}}{\partial t} + \rho \mathbf{v} \cdot \bigtriangledown \mathbf{v} = \sum_j f_j \tag{2.3}$$

This is the most basic form of the Navier-Stokes equation. From here on out $\mathbf{v}(r(t),t)$ will be written as just $\mathbf{v}$ for clarity. The sum of force densities on the right side of equation (2.3) can be examined further. It includes all the force densities acting on the system. The pressure-gradient force density and the viscous force density must be taken into account. The pressure-gradient force density depicts the pressure exerted by the volume S on its surroundings, while the viscous force density outlines the frictional forces with the surroundings the volume S is subject to. For an in-compressible liquid these are given by

$$f_p = - \bigtriangledown p \tag{2.4a}$$

$$f_{visc} = \mu \bigtriangledown^2 \mathbf{v} \tag{2.4b}$$

The minus sine in equation (2.4a) is factored there, because now the equation represents force densities acting on the system. Then, $\sum_j f_j$ will result in

$$\rho \frac{\partial \mathbf{v}}{\partial t} + \rho \mathbf{v} \cdot \bigtriangledown \mathbf{v} = \mu \bigtriangledown^2 \mathbf{v} - \bigtriangledown p + \sum_{ext} f_{ext} \tag{2.5}$$

with $\sum_{ext} f_{ext}$ the summation of any external force densities possibly acting on the system.

2.2 Deriving flow behaviour inside a channel through Navier-Stokes

Flow dynamics through a channel are one of the few processes that can be solved analytically. This is because the channel gives rise to several boundary conditions, simplifying the Navier-Stokes equations. For a horizontal pipe, gravitational forces will be cancelled out due to the hydro-static pressure inside the pipe. In this experiment, no other external forces will be applied to the system. Thus, the sum of external forces in equation (2.5) can be neglected.

One major assumption for fluid dynamics inside a channel is the no slip boundary condition. It states that on a molecular level, the molecules of the fluid that are next to the boundary will have no velocity relative to the boundary.

$$\mathbf{v}(r) = 0, for \qquad r \in \delta S_b \tag{2.6}$$

Where δS_b is the location of the boundary.

Microfluidics is a regime where velocities are typically small. This results in inertial forces that are small compared to the viscous forces. Inertial forces are forces due to the momentum of the fluid, and the main source of turbulence inside a channel. Thus, microfluidics occupy a range of extremely laminar flow. The Reynolds number is a number that gives the ratio of inertial forces to viscous forces inside a boundary layer, and is used as a measure for the turbulence in a channel. It is given by

$$Re = \frac{D_h \rho < v >}{\mu} \tag{2.7}$$

with D_h the hydraulic diameter of the microchannel and $< v >$ the average velocity inside the channel. If the inertial forces are small compared to the viscous forces, this means that $Re << 1$. Flow rates are in the range of $\mu l/min$, and channel diameters typically range from $1-100\mu m$[9]. This causes non-linear velocity terms to vanish in the Navier-Stokes equations, resulting in

$$\rho \frac{\partial \mathbf{v}}{\partial t} = \mu \bigtriangledown^2 \mathbf{v} - \bigtriangledown p \tag{2.8}$$

This is known as the Stokes-equation. This can be examined further for flow inside a channel.

If one chooses the x-axis is parallel to the channel the y-axis and z-axis parallel to the cross section of the channel, the flow velocity inside the channel doesn't change in the x-direction, and since the flow is extremely laminar, no flow velocity will be in the y-direction or z-direction. Thus the velocity does not change over time, leaving

$$\mu \bigtriangledown^2 \mathbf{v} = \bigtriangledown p \tag{2.9}$$

From these assumptions, one can also conclude that the velocity field only has a component in the x-direction, but that this component is independent of

translation in the x-direction. This also means that the pressure changes only occur in the x-direction. The no slip boundary condition defines a dependency in the y-direction and z-direction, leaving

$$p(\mathbf{r}) = p(x) \tag{2.10a}$$

$$\mathbf{v}(r) = v_x(y,z)\hat{x} \tag{2.10b}$$

Assuming that the pressure drops linearly, starting with a pressure p_0 and having a total pressure drop of Δp, one finds

$$p(x) = \frac{\Delta p}{L}(L-x) + p_0 \tag{2.11}$$

with L the length of the channel.

With the no slip boundary condition (2.6), the resulting derivation of equation (2.9) is solvable for any symmetrical cross section S.

$$(\partial_y^2 + \partial_z^2)\mathbf{v}_x(y,z) = -\frac{\Delta p}{\mu L}, \qquad for \quad y,z \in \delta S \tag{2.12a}$$

$$\mathbf{v}_x(y,z) = 0, \qquad for \quad y,z \in \delta S_b \tag{2.12b}$$

equation (2.12a) shows that the pressure drop in a channel is linearly dependant on the viscosity of the liquid phase. The pressure drop over a length x will decrease as a liquid phase has a higher viscosity. This is an important characteristic in pressure driven flow, and plays an important part in two phased flow.

2.3 Capillary effects

When $Re << 1$, inertial forces are neglible compared to the viscous forces inside the channel. However, the viscous forces are not the only force acting on the system. Another important factor to examine in microfluidics is the surface tension of two immiscible organic- and aqueous phases and the boundaries. It's a phenomenon that strives to minimize the surface area of a particular fluid's surface that is in contact with another fluid, or a gas or solid.

Inside a liquid, there are cohesive forces between molecules. If a molecule is fully surrounded by the same molecules, the forces are symmetrical, leading to an equilibrium of forces. However, at the boundary, this equilibrium cannot persist. The molecules at the very boundary still have cohesive forces of neighbouring molecules, but also have a different cohesive force with the molecules in the different medium. This results in a net force pulling the molecule away from the boundary. This is shown schematically in figure (1).

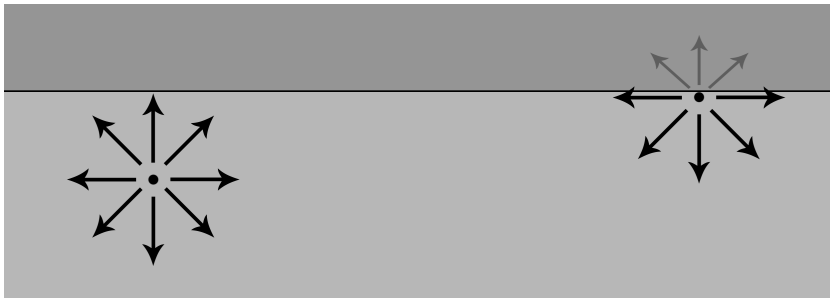

Figure 1: Schematic representation of surface tension forces acting on a molecule. The boundary between the interfaces is shown as the black line. The dark gray mass above the boundary is either a solid or a liquid, the lighter gray depicts a liquid. The arrows represent cohesive forces between the molecules and their neighbouring molecules.

The molecule at the interface creates an internal pressure, with its surplus free energy [10]. If the surface of the interface is minimal, there is a minimal amount of molecules will have free energy generating pressure for the liquid, thus the system is at its most stable with a minimal area. This is one reason circular droplets are formed in two phased flow with two immiscible liquids. A sphere has the lowest surface to volume ratio, thus is the most stable form for the droplet. One important dimensionless number used in microfluidics is the Capillary number. It gives the ratio between the viscous force and the surface tension force

$$Ca = \frac{\mu V}{\gamma} \tag{2.13}$$

In a microchannel, surface tension effects become more prevalent, due to the small channel dimensions [18] [8].

2.4 Surface tension and Young-Laplace pressure

The above paragraph discusses the interaction at the boundary between two immiscible liquid phases, or between a liquid phase and a solid. When looking at two immiscible liquid phases the surface tension has an important consequence. It generates a curved interface between the phases, as a product of the Young-Laplace pressure. In the case of a free surface, the Young-Laplace pressure is given by [13]

$$\Delta p = \gamma(\frac{1}{R_1} + \frac{1}{R_2}) \tag{2.14}$$

where γ is the surface tension, and R_1 and R_2 are the radii of the curved boundary. However, inside a bounded area, like for instance a microchannel with two phase parallel flow, there is only one radius present, resulting in

$$\Delta p = \frac{\gamma}{R} \tag{2.15}$$

This radius will have a contact angle with the boundary of a microchannel. This contact angle is a direct indication of the surface tensions between the two liquids and the boundary

$$\cos\theta = \frac{\gamma_{sl_2} - \gamma_{sl_1}}{\gamma_{l_1 l_2}} \tag{2.16}$$

This is called the Young equation [12]. The contact angle between a solid and an aqueous phase is a measure of the hydrophobicity of the surface. If they have a contact angle $\theta > \pi$, the solid is hydrophobic, or has a low wettability.

A schematic representation of the contact angle is shown in figure (2). The figure is a cross-section of a rectangular microchannel with two liquids flowing through it.

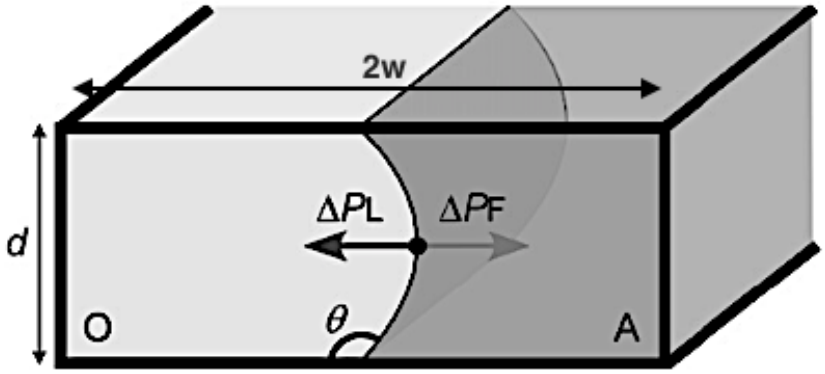

Figure 2: A schematic representation of the Laplace pressure and the contact angle in a rectangular microchannel with two liquids flowing through it[14].

In the figure, a distinction is made between the organic phase and the aqueous phase, denoted by A and O respectively. d is the depth of the channel, and w is the half width. It also shows the location and direction of the Laplace pressure ΔP_L and the viscous pressure ΔP_F. The viscous pressure is a pressure difference between two phases with different viscosities and velocities, a product of shear stress. These pressures balance each other out, in the case of a stable interface [14].

Surface tension forces play a major role in microfluidics. One way to minimize the effect of forces perpendicular to the flow of the phases, is the application of surface modifications to a microchannel[17][19]. Microchannel walls have been coated with a hydrophobic coating to provide more stable parallel flow, since the interface itself is restricted in its movement in the direction perpendicular to the flow[14]. A hydrophobic surface layer prevents the aqueous phase from attaching. When a portion of the channel is coated where the organic phase resides, the aqueous phase will be limited in its motion towards that part of the channel. This prevents interface collapse due to wetting of the channel.

2.5 Two-phase flow

Several processes have been introduced that describe interactions between two phases inside a channel. However, flow inside a channel has only been discussed for one phase so far. In this section the steady state parallel flow of two immiscible liquid phases inside a microchannel will be discussed. Two phase flow resembles one phase flow through a channel, however, it has to take into account some extra variables and processes. The Laplace pressure and the viscous pressure discussed above are two of these. They give the boundary conditions of where the interface between two phases will manifest itself inside the channel. In figure (3), two phased parallel flow is shown. The interface resides at width $z = h^*$.

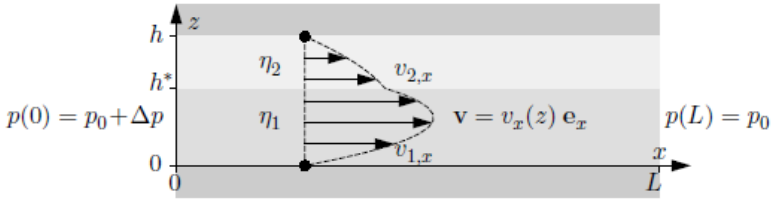

Figure 3: a schematic representation of a two-phase flow microchannel for two liquid phases with respective viscosities η_1 and η_2. In this case, $\eta_2 > \eta_1$ [10]

.

In this figure, multiple processes are summarized. For one, it shows the pressure drop of both liquids inside the channel. Here the overall pressure drop is constant for both liquid phases. Liquid phase 2 will have a lower velocity at

the same pressure drop, because it has a higher viscosity, as shown in equation (2.12a). This results in a shear stress at the interface between the two phases, which generates the viscous pressure that was discussed in subsection 2.4. Both liquid phase 1 and 2 must experience the same shear stress at the interface, and both are still subject to the no slip boundary condition equation (2.6) at the interface, but also at the boundary. This results in the following boundary conditions for continuous parallel two-phase flow

$$v_2, x(h) = 0 \tag{2.17a}$$

$$v_1, x(0) = 0 \tag{2.17b}$$

$$v_1, x(h^*) = v_2, x(h^*) \tag{2.17c}$$

$$\sigma_1, x(h^*) = \sigma_2, x(h^*) \tag{2.17d}$$

The interface location h^* is deemed important in generating no leakage parallel flow. The assumption is made that if the interface is formed at width $h^* = \frac{1}{2}h$, both phases will split off at width $h^* = \frac{1}{2}h$ at the outlet of the channel. This would result in pure phase separation, without leakage from either phase towards the other phase outlet. This is assumed on the basis of the stability of the highly laminar flow inside a microchannel. For clarity, h^* and h are from here on out referred to as width w^* and w.

In order to have parallel flow established at $w^* = \frac{1}{2}w$, at the halfwidth of the channel, the ratio between flow rates needs to be proportional to the ratio of the viscosities of the used phases

$$\frac{Q_1}{Q_2} = (\frac{\mu_1}{\mu_2})^{-0.76} \tag{2.18}$$

This formula was found experimentally by Pohar *et al.*[16], in a microchannel with a y-junction inlet but a single outlet channel. It is not directly applicable to the y-junction inlet, y-junction outlet channel, but it does give a framework of establishing parallel flow with an interface width of $w^* = \frac{1}{2}w$.

2.6 Flow patterns

Based on the transition limits of the Reynolds number and the capillary number, three regimes can be distinguished. One regime where surface tension forces will be dominant over the viscous forces and inertial forces in the system, one regime where inertial forces are the dominant forces in the system, as is the case with turbulent flow, and one transition regime. In this transition regime, several flow patterns can be described. The behaviour of two-phase flow and the corresponding flow patterns have been a field of interest for various research groups [14] [15] [18].

These patterns are shown in figure (4). For this research, double y-junction chips were examined. in favor of T-junction chips, because the y-shaped inlet is beneficial to the stability of parallel flow [22].

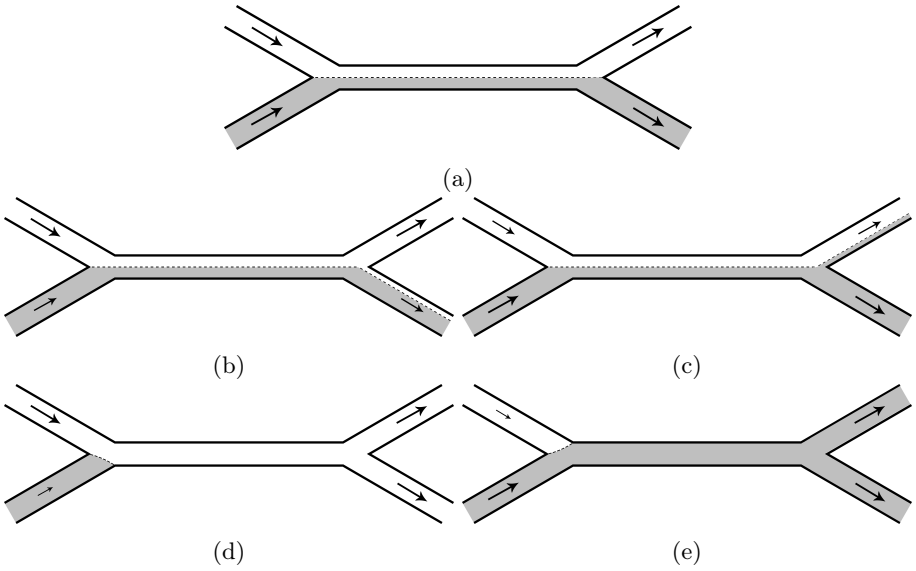

Figure 4: This figure depicts several possible flow patterns inside a microchannel. (a) no-leakage parallel flow. (b) parallel flow with aqueous leakage into organic outlet. (c) parallel flow with organic leakage into aqueous outlet. (d) organic droplet flow inside aqueous phase with cut-off at inlet. (e) aqueous droplet flow inside organic phase with cut-off at inlet.

The vectors in the figure outline the direction of the flow, as well as their relative velocity. There is a dotted line present indicating the interface of the channel. The gray liquid represents the organic phase, while the white liquid represents the aqueous phase. For each flow pattern, it is assumed that the viscosity of the organic phase is lower than the viscosity of the the aqueous phase.

The first flow pattern, figure (4a), is the no-leakage parallel flow. Here, The interface height equals $w^* = \frac{1}{2}w$. The Reynolds numbers are in the same order

of magnitude, their ratio given by equation (2.18) and there is no substantial wetting present. The viscous force will be dominant over the surface tension force, otherwise droplet flow would occur. Figure (4b) and (4c) show leakages at the outlet of the channel. Here, it is assumed that $w^* = \frac{1}{2}w$ still holds. Thus, the leakages could be caused by a deviation in viscous stresses due to high viscosity discrepancies, or by surface tensions of either liquid phase with the boundary. Figure (4d) and (4e) show non parallel flow patterns. They depict droplet flow inside a channel. With droplet flow, it is expected that the interface will not establish at $w^* = \frac{1}{2}w$, or not establish at all. Figure (4d) and (4e) show the extreme case, where either flow is cut off due to extreme flow rate ratios and droplet flow initiates at the inlet of either channel. If the liquid phase that was cut off is the liquid that wets the channel, slug flow will form. Otherwise, mono-dispersed droplets will flow through the center of the channel, without any contact with the channel boundaries[18].

One last flow pattern that can be observed is annular flow [18]. annular flow forms when a surface has a high wettability with either phase, and the phases have Reynolds numbers that would allow parallel flow. In the figure below, the aqueous phase will form a layer between the hydrophilic boundary of the channel and the organic phase, and the organic phase will form parallel flow around the middle of the channel, because of its hydrophobicity.

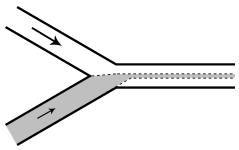

Figure 5: This figure is a schematic representation of annular flow within a microchannel.

Since Zhao *et al.* [18] did not use a double y-channel, the outlet of the flow can not be drawn with certainty. In the most stable case, the organic phase will enter both the organic outlet and the aqueous outlet, causing both outlets to experience leakage.

3 Experimental Method

3.1 Experimental Set-up

This subsection will give an overview of the experimental set-up used, to provide context for the following subsections, discussing the variable changes, figure (6) shows the set-up of this research schematically.

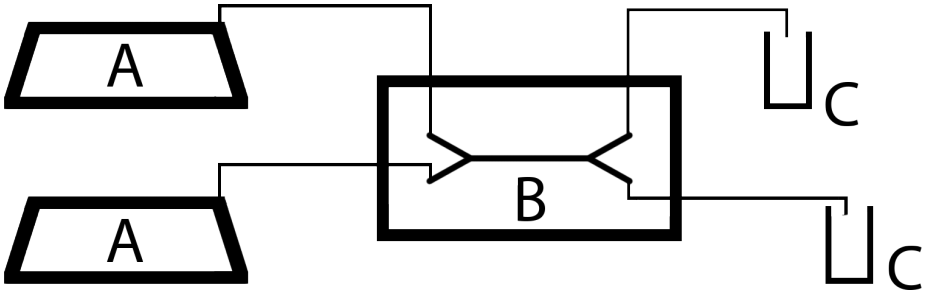

Figure 6: This schematic figure depicts the experimental setup of this research. The pumps are denoted by A, the chip is denoted by B, and the outlets are denoted by C.

Two syringe pumps, denoted by A in figure (6), were used to pump the liquids phases into the microchannel, denoted by B. The outlet is connected to two glass vials, denoted by C. The tubing connecting the pump, the chip and the outlet was made out of teflon and had an inner diameter of $0.5mm$. It was produced by IDEX. The tube length from the pumps to the chip was $10cm$. The tube length from the chip to the outlets was $30cm$.

The chip was examined through a microscope. It made use of lighting where the chip was situated, to provide a more clear view of the microchannels.

The bottom pump of figure (6) was used for organic phases, while the top pump was used for aqueous phases. This resulted in a view through the microscope that was equivalent to figure (4), with organic phase in the bottom part of the channel and aqueous phase in the top part of the channel.

For the analysis of parallel flow, the set-up was altered in three different ways. Three organic phases were injected through two different microchannel chips which were examined at changing flow rates of the aqueous and the organic phases through the channel. Temperature, height of the inlet and outlet and tube length were variables that were kept constant. In the following subsections each of the three set-up changes will be discussed, together with their respective variable changes.

3.2 Chips

Two different microchannel chips were used. Both chips were double y-junction chips, with two inlet-channels and two outlet-channels. One chip was manufactured by the Institute of Microchemical Technology (IMT). The chip in question was the ICC-DY15G. The other chip was manufactured by MICRONIT Microtechnologies, the MICRONIT Microreactor H300.015.2. These chips will be referred to as the IMT chip and the Micronit chip respectively. Changing the chips was primarily done for the effect of the shape and dimensions of the channel on parallel flow. This has an effect on the pressure through the tubing, but also on the flow velocity, thus impacting the Reynolds number and Capillary number. The dimensions of the chips are given in table 1.

Table 1: This table depicts the dimensions of each chip used.

Chip	Depth (in μm)	Width (in μm)	Channel length (in mm)
IMT chip	40	100	120
Micronit chip	150	300	14.8

Note the difference in reactor channel length of the channel. This is the length of the channel where the two phases interact, between the y-junctions. The length of the channel is an important factor in pressure driven flow, and should be kept constant in able to recreate a comparable analysis on other variables for both chips. A length difference of $105.2mm$ is equal to a 20% percent increase in channel length. Thus, this is a variable that should be taken into account when analyzing differences between the chips.

The chips did not have the same cross section. While the Micronit chip has a shape that resembles a wide parabola. the IMT chip has a unique shape. Its channels are separated by a wedge. The IMT company calls it a guide structure. It promotes parallel flow stabilization [23]. The guide structure in the channel decreases the depth of the channel at the location of the interface, which allows a larger contact angle range, thus increasing the stability of the interface [14].

When switching the chip, a change in surface tension between the organic and aqueous phase with the solid boundary can occur. Because the chips are manufactured by a different company, their surface tension will not be exactly equal, even if they are manufactured from the same material. The wettability of a channel changes with the roughness of the channel [24]. This could play a role in the behaviour of the phases inside the chip. Both chips are made of borosilicate glass, which is a hydrophilic glass with a contact angle with water of 32^o [20].

3.3 Pump

The pumps used were AL-1000 pumps manufactured by Aladdin. $5mm$ syringes were installed into the pumps. The syringes were manufactured by B-D, and had an inside diameter of $11.99mm$, which had to be taken into account when setting up the pumps. The pumps were used to control the flow rate within the channel. They are shown in table 2.

Table 2: This table depicts the minimum and maximum flow rates of each pump used.

Name pump	ϕ_{min} (in $\mu l/min$)	ϕ_{max} (in $\mu l/min$)
Pump IMT	10	50
Pump Micronit	0.079	5760

Here, ϕ_{min} and ϕ_{max} represent the minimum and maximal flow rates the pump could generate. The first pump was used with the IMT chip, while the second pump was used with the Micronit chip. The limit on the IMT chip pump was not due to the maximal limits set by the company, but because of the limits that were set up on the specific pump electronically. This limited IMT measurements. The limit on the Micronit was a function of the syringe volume and inner diameter, and given in the Aladdin instruction manual.

3.4 Organic phases

Three different organic phases were used. All three were produced by SIGMA-ALDRICH. The organic phases were chosen mostly on the basis of viscosity differences. Viscosity differences between two phases in two phase flow will give rise to pressure differences at the interface, as shown in (2.12a). Equation (2.18) also predicts a ratio of flow rates for a set viscosity difference in order to establish an interface at $w^* = \frac{1}{2}w$. Table (3) depicts the viscosity of each of the three chosen organic phases, as well as their densities and interfacial tensions.

Table 3: This table depicts the significant chemical properties of each organic phase.

Organic phase	Viscosity (in $mPas$)	Purity	$\gamma_{o,a}$ (in mJ/m^2)
Decane	0.92	$\geq$ 95 %	52.33 [26]
Heptane	0.386	99 %	51.24 [26]
Toluene	0.59	99.4 %	37.1 [27]

All properties were taken at room temperature 20^oC. Decane was chosen due to its similar viscosity to water. Heptane is dissimilar in viscosity to water, thus it was chosen to see the effects of high viscosity differences between the two phases. Toluene could be used to explain surface tension effects in the channel.

3.5 Silanization

One option to modify the surface layer of the boundary of a microchannel in order to stabilize parallel flow inside a microchannel is silanization with an organosilane. Silanization attaches an organosilane to the surface. the reactive end of the organosilane bonds to the surface while the tail end becomes the dominant surface chemical. If a tail end is chosen with highly hydrophobic chemical properties, surface tension effects can be altered inside the channel.

Octadecyltrichlorosilane (OTS) was chosen as the silanization reagent. OTS has three reactive chloride groups and a long 18-carbon tail. The chloride atoms react with trace amounts of water and are replaced with hydroxyl groups to form silanol groups with elimination of hydrochloric acid. These silanol groups engage in condensation reactions with the silanol groups present on the surface of the glass, as well as with silanol groups of other OTS molecules, forming covalent silanol bonds. This way a self-assembled monolayer can be formed on the glass surface [21]. This is shown schematically in figure (7).

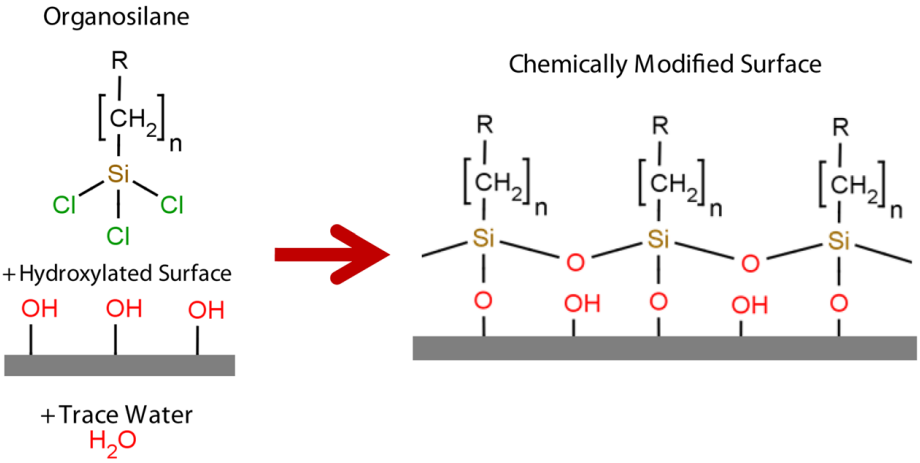

Figure 7: With silanization, an organosilane attaches to the surface. The tail end of the organosilane becomes the dominant surface chemical species[21].

The coating process was guided by a method introduced by Rob Wenmaekers, which he developed for his Master's Thesis. It is outlined in table (4). It is based on various examples in literature, Glass *et al.* [21] and Hirama *et al.* [25] and on the possibilities within the lab.

Table 4: This table shows the procedure required to effectively coat a microchannel with a hydrophobic layer through silanization.

Step	procedure	material	duration
1.	Rinse	milliQ water	2 min.
2.	Hydroxylate surface	1M HCl	5 min.
3.	Dry	Filtered air	5 min.
4.	Rinse	toluene	2 min.
5.	Silanization	1% OTS in toluene	30 min.
6.	Rinse	ethanol	5 min.
7.	Rinse	milliQ water	5 min.

All the steps were carried out at $50\mu l/min$ with both syringes, except for step 5. Since only part of the channel had to be coated, The OTS solution had a lower flow rate, compared to the toluene coming out of the other channel. This ensured that the OTS solution would not travel past halfway through the channel. The flow rates chosen were $30\mu l/min$ for the OTS solution, and $90\mu l/min$ for the pure toluene. the latter was chosen to minimize diffusion of OTS to the other side of the channel.

4 Results and Discussion

4.1 IMT chip

4.1.1 IMT flow pattern plot analysis

A general insight in parallel flow inside a microchannel was the starting point of this project. This was done with flow pattern plots, examining various flow rate ratios. Below, in figure (8), the flow pattern plot of the organic phase decane and the aqueous phase is shown for the IMT chip. For this range, $10\mu l/min - 50\mu l/min$, it showed all the possible two-phase flow options surrounding parallel flow except annular flow. These are given again in the legend of the figure.

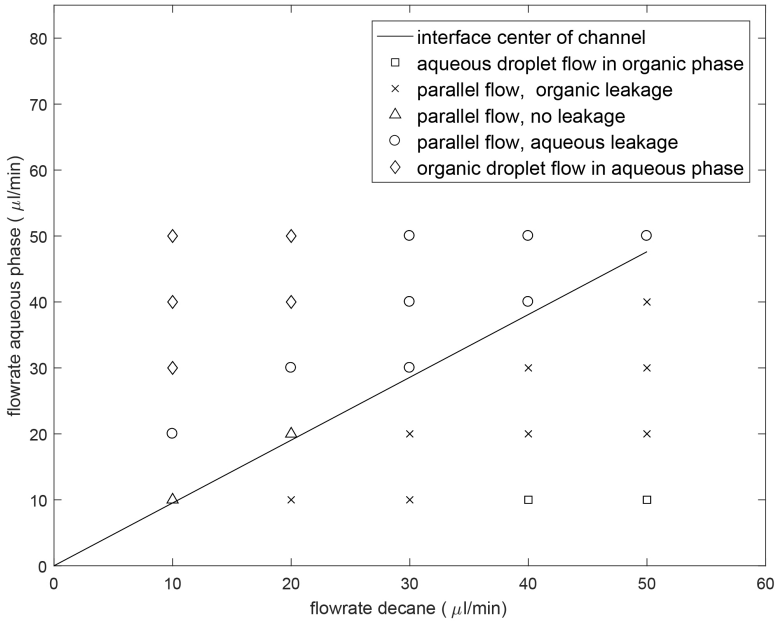

Figure 8: A plot of various flow ratio's between decane and water. *parallel flow, aqueous leakage* denotes the flow pattern discussed in figure (4b), while *parallel flow, organic leakage* denotes the flow pattern discussed in figure (4c).

Decane has a viscosity closest to water, relative to the other organic phases used, so their relative flow rate is closest to 1 for a centered interface, as described by Pohar *et al.* in equation (2.18) [16]. This proposed ratio is represented by the line through the flow pattern plot. When the relative flow rate was near the centered interface equilibrium, leakage to either side appeared to minimalize. High relative flow rates resulted in a cut-off at either phase, resulting in droplet flow. Thus, the different two-phase flow possibilities were behaving as described

by the theory.

While the two-phase flow behaved similar to the theory's predictions, it was apparent that aqueous leakage seemed to appear more frequently than organic leakage. For instance, where no leakage parallel flow was expected, slight aqueous leakage occurred. While doing measurements, the organic channel seemed to be wetted by the aqueous phase, allowing for a lower threshold for aqueous leakage into the organic phase to occur. This was also prevalent when leakage occurred in general. Organic leakage into the aqueous outlet manifested itself as droplet flow, while aqueous leakage into the organic outlet flowed parallel to the organic phase. The wetting of the organic outlet can be seen in the figure (9), which is a photo taken of the process. Small aqueous bubbles arose in the organic phase. This phenomenon increased with aqueous flow rate, which is in line with the non-leakage parallel flow disappearing with higher flow rates.

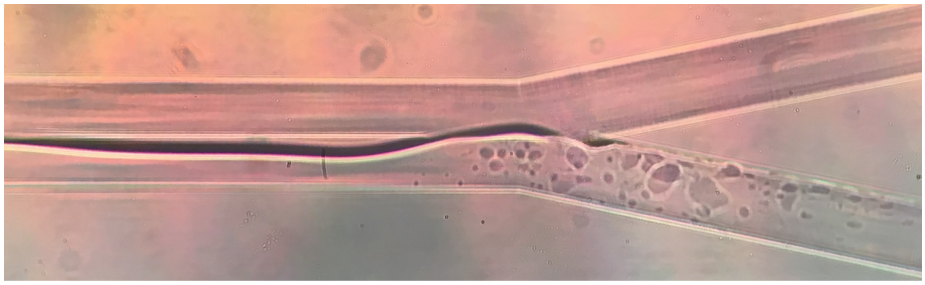

Figure 9: A photo showing the wetting of the organic channel by the aqueous phase, making aqueous leakage into the organic outlet more plausible. It was taken at a flow rate of $30\mu l/min$ for both the organic and the aqueous phase. The organic phase depicted is decane.

Parallel flow without any leakage did occur in the case of decane, but only in the lower flow rate ranges. Here, the wetting was less prevalent, which allowed the parallel flow to stabilize longer. Indefinite stabilization of no leakage parallel flow did not occur. Perturbation in the pumps and inertial forces could be the explanation of the instability of the parallel leakage. Table (5) shows that the minimum Reynolds number was slightly above 1, and the maximum Reynolds numbers observed in this experiment were well above 1 for the IMT chip. This means inertial forces were not negligible.

Table 5: This table depicts the range of Reynolds numbers and capillary numbers observed inside the IMT glass chip.

phases	Re_{min}	Re_{max}	$Ca_{min} \times 10^{-3}$	$Ca_{max} \times 10^{-3}$
Water	3.7	19	-	-
Decane	3.0	15	0.73	3.7
Toluene	5.5	27	0.66	3.3
Heptane	6.4	32	0.31	1.6

It can be concluded that the Stokes flow derivation cannot hold in this case, since it required $Re << 1$. This could mean that the equilibrium between the Laplace-pressure and the viscous forces is impacted, because the inertial forces would cause instability. This could give rise to interface collapse, thus allowing the wetting of the channel. Slight annular flow would occur, guaranteeing aqueous leakage into the organic phase outlet. In table (5), the range of capillary numbers for the IMT chip is also shown. In this range, capillary effects are not negligible, since droplet flow was detected. However, figure (8) showed that changing the flow ratios still had a dominant impact on the flow patterns.

The results did not contradict for all three organic phases. The flow pattern plot figures for heptane and toluene are in the Appendix. Increasing the aqueous flow rate above the proposed ratio gave rise to organic leakage into the aqueous outlet, and decreasing it resulted in aqueous leakage. This process can be examined further when looking at relative flow rates more closely. R_f is defined as the ratio between the organic phase and the aqueous phase Q_{org}/Q_{aq}, and is expressed in figure (10).

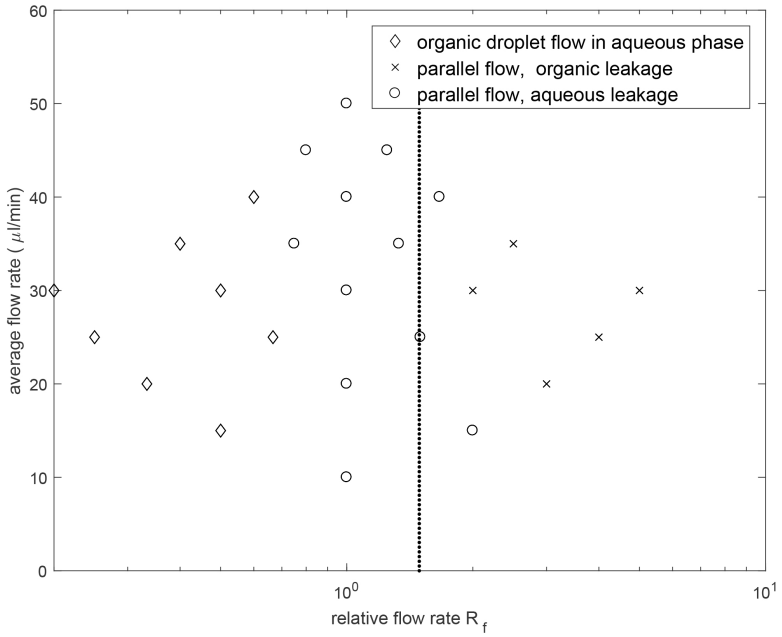

Figure 10: A plot of the average flow rate through a channel compared to the relative flow rates, depicting the flow patterns present. This plot compares toluene to the aqueous phase.

Various conclusions can be deduced from this plot. The transition between organic leakage and aqueous leakage, flow patterns shown in figure (4c) and

figure (4b) in subsection (4), occurs at a flow rate ratio required for a centered interface. This is another indication that an interface at $w^* = \frac{1}{2}w$ is highly important for no leakage parallel flow, or NLPF, inside a double y-channel.

Furthermore, the flow pattern present in the microchannel is dependant on the relative flow rate. This can be deduced due to the fact that the flow pattern changes steadily as toluene's flow rate is increased compared to the aqueous phase. The flow rate ratio in itself does not represent any force acting on the channel. The forces responsible for this behaviour are the viscous forces at the interface. Equation (2.12a) shows that in one phase flow, the pressure drop over the length of the channel $\Delta p(x)$ is linearly dependent on the viscosity μ and the velocity of the liquid phase $v(x)$. Subsection (2.4) and (2.5) introduced the difference in this pressure between the two liquid phases as viscous forces. If the relative pressure at the outlet is large enough, and the interface roughly resides at $w^* = \frac{1}{2}w$, the interface will be dislocated from the outlet of the channel and leakage will occur. The relative pressure at the outlet is the ratio between the pressure of the organic phase at the outlet versus the pressure of the aqueous phase at the outlet and is only dependant on the viscosity ratios and the velocity ratios, since microchannel dimensions cancel out in the case of $w^* = \frac{1}{2}w$. This relative pressure will be denoted as R_p.

When analyzing the flow patterns further, the results from all three organic phases could be compared. Figure (11) shows a comparison between all three organic phases.

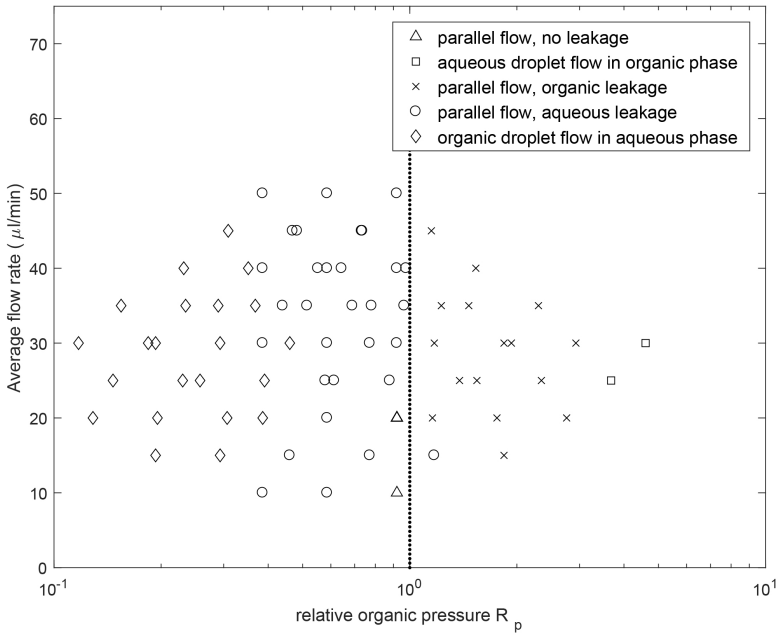

Figure 11: A figure showing the distribution of flow patterns for the average flow rate versus the relative pressure R_p they were observed at.

A clear correlation between the relative pressure and the flow pattern is observed. Figure (11) also shows where equation (2.18) originated. Where previously the transition from organic leakage to aqueous leakage occurred at that relative flow fraction, figure (11) shows that this transition now occurs at a relative pressure of 1. In other words, if the two phases are driven by an equal pressure, NLPF will be most likely.

4.1.2 IMT NLPF

This does raise one question. In the flow pattern plots, no-leakage parallel flow was only found sparsely. The flow pattern plots did help to narrow down the regions inhabited by flow patterns. In the the region of pressure equilibrium, NLPF was found for each organic phase in the same region of flow rates, $10\mu l/min - 50\mu l/min$. It is important to note that while brief NLPF was observed, the interface did not stabilize long. Again, this is accounted to the pertubation of the pump, and the slight inertial forces impacting the flowrates. The values of this short term NLPF are shown in figure (12), which is a version of figure (11), zoomed in to the pressure equilibrium.

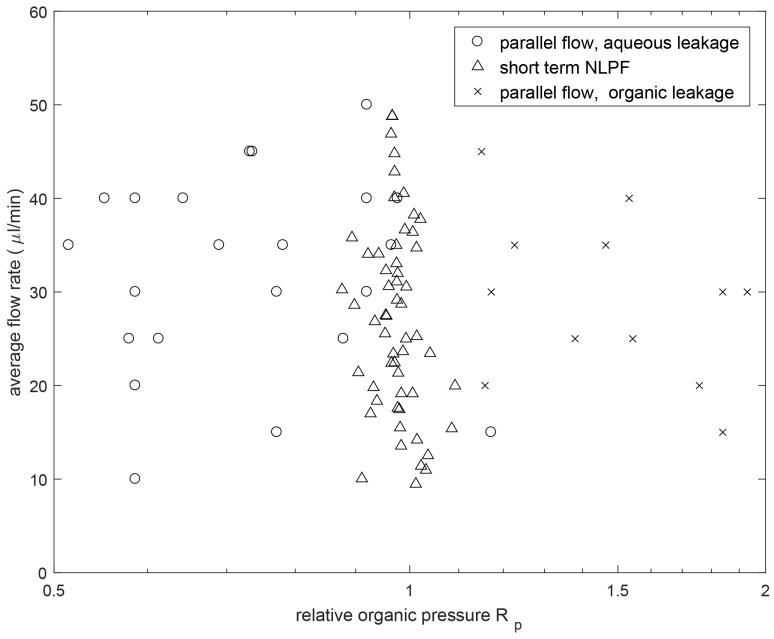

Figure 12: This figure shows the location of short term NLPF within the flow pattern analysis. Here, × depicts organic leakage, △ depicts short term NLPF and ∘ depicts aqueous leakage.

As seen on the scale, short term NLPF found was in the region of $0.9 - 1.1R_p$, between the transition from organic leakage to aqueous leakage. The total Reynolds number does not seem to impact the short term stabilization of NLPF. Outside of this region, it was impossible for all three organic phases to establish NLPF, because the pressure difference would push the interface off $w^* = \frac{1}{2}w$ at the outlet, resulting in leakage. Through this, together with the correlation between relative pressure and flow patterns determined shown in figure (11), it can be concluded that viscous forces are the dominant factor in determining flow patterns in this regime, if the interface stabilizes itself roughly at width $w^* = \frac{1}{2}w$. However, the surface tension force and the inertial forces still impact the stability of the interface and flow patterns in this regime.

4.2 Micronit chip

4.2.1 Micronit flow pattern plot analysis

With the IMT chip, most processes that interact with the ability of a two-phase flow to stabilize into parallel flow were examined and discussed. The goal of further research with the Micronit chip is twofold. On the one hand, the observations with the Micronit chip could be used to solidify the already standing arguments presented with the IMT chip. On the other hand, it could be used to explain processes the IMT-chip data was insufficient for, or prove theorems that arose while looking at the IMT-chip. Examining extremities in two-phase flow is an example of the former, the effect of the wettability of the channel and persistent aqueous leakage into the organic phase outlet, which will be discussed later, are examples of the latter.

When evaluating the Micronit chip, a different pump could be used, which allowed for higher flow rates. This also meant that higher flow rate ratios could be examined. This was done with another flow pattern plot, this time ranging from $10\mu l/min$ to $90\mu l/min$. Higher than $90\mu l/min$ was not desirable, because of the implications a higher Reynolds number would bring. Because of the dimensions of the Micronit chip, higher flow rates could be used without going into even higher Reynolds regimes. Its results are shown in figure (13).

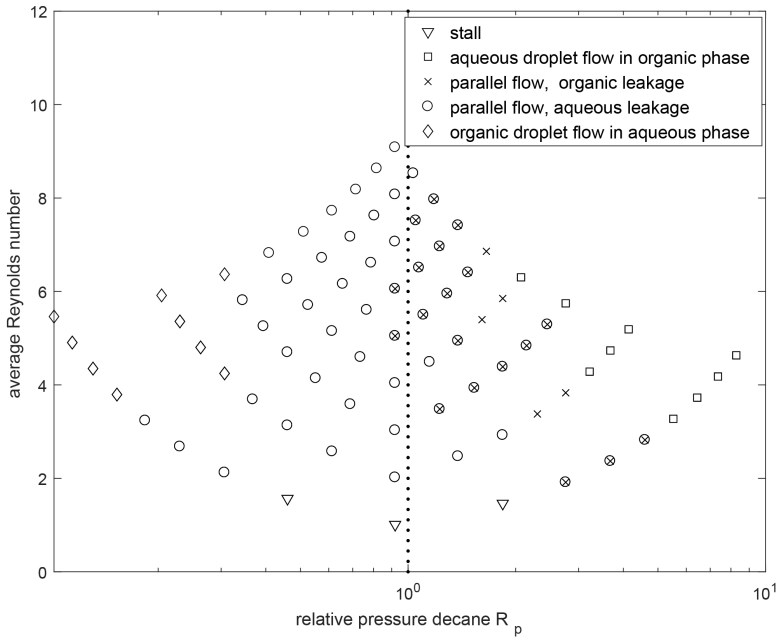

Figure 13: A plot depicting the flow patterns distribution for a relative pressure R_p between decane and water for the Micronit chip.

Again, the transition between organic leakage and aqueous leakage occurs at $R_p = 1$, even though NLPF is absent.

With the Micronit chip, a new phenomenon is observed. Where the IMT chip did not show simultaneous aqueous and organic leakage, the Micronit chip almost always had some form of aqueous leakage into the organic outlet. This made NLPF impossible in the Micronit chip. As seen in figure (13), only at high pressure differences did aqueous leakage not occur. Even then, the flow pattern quickly transitioned into aqueous droplet flow. The process of double leakage is shown in figure (14). It is a photo taken through the microscope at an organic flow rate of $80\mu l/min$ and an aqueous flow rate of $60\mu l/min$, altered slightly so both leakages could be visible.

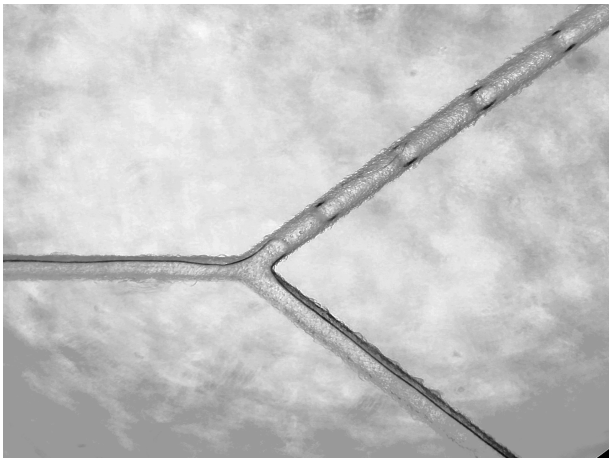

Figure 14: A photo of the Micronit chip, where both organic and aqueous leakage are present simultaneously. The decane outlet is situated in the bottom side, while the aqueous phase exits the top outlet.

One explanation for this could be the roughness of the Micronit channel increasing its wettability. The Micronit chip was of lesser quality than the IMT chip. This could be seen clearly when looking at the smoothness of the boundaries of the chips through the microscope, and it can be seen by comparing figure (9) and figure (14). The photo also shows us that organic phase leakage was in the form of droplet flow, while aqueous phase leaked parallely to the channel. This can be explained by the wettability of the chip. Borosilicate glass is hydrophilic in nature, thus the aqueous phase will manifest itself easier on the boundary than the organic phase, which is more likely to produce as little contact as possible with the boundary.

4.2.2 IMT and Micronit comparison

The IMT chip and the Micronit chip were hard to compare. The channel dimensions are dissimilar, but the flow rates are in the same order of magnitude. This results in a pressure present at the IMT chip outlet in the order of $p = 10^5$. This was at a factor 10^2 higher than at the Micronit chip outlet, which only had a pressure at the outlet in the order of 10^3, since their cross section areas differ approximately by a factor 10, see table (1) in subsection (3.2). The pressure at the outlet was calculated using equation (2.12a) and approximating both channels as a rectangular channel. Despite the pressure differences, both systems show the same behaviour approximately. One difference that is apparent is the stall in the Micronit chip, which is not observed in the IMT chip. Thus, the stall in the Micronit chip could be a product of the low pressure inside the microchannel. A major increase in total pressure at the outlet does not change the flow pattern behaviour directly. The total pressure at the outlet could affect the stability of the interface. Due to the lower pressure observed at the outlet in the Micronit chip, the interface was able to move more freely with perturbation, increasing the instability of the channel.

4.3 OTS coating

The lesser quality of the Micronit chip could have impacted the wettability of the channel boundaries. This was counteracted by coating the chip with an organosilane with a hydrophobic tail end, as discussed in subsection (3.5). This proved to be highly successful. In figure (13), aqueous and organic droplet flow and stalling could be examined. The relative pressure plot of the OTS-coated Micronit chip, figure (15), shows a comparative exceptionally stable parallel flow.

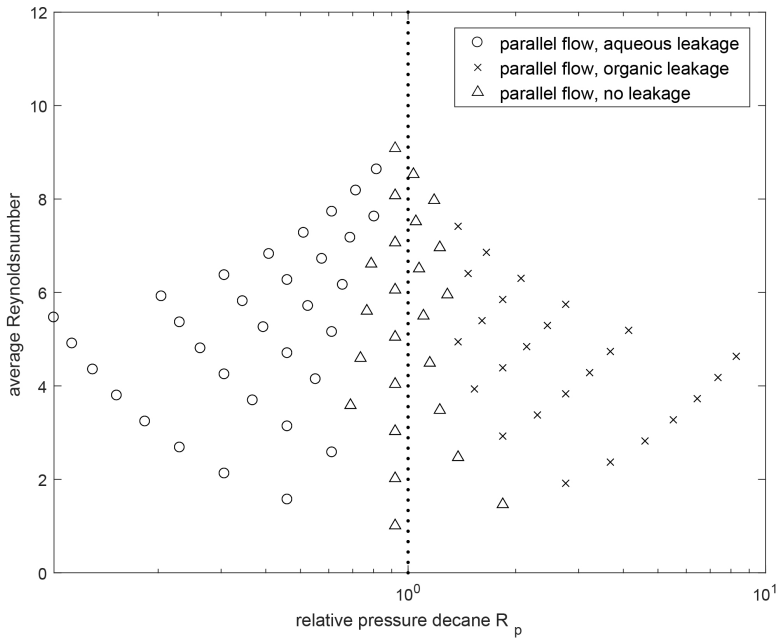

Figure 15: A plot depicting the flow patterns distribution for a relative pressure R_p between decane and water for the OTS coated Micronit chip.

Even at extreme pressure drop ratios R_p, parallel flow persists in the OTS coated Micronit chip, from here on referred to as OTS chip. NLPF situates itself around the pressure equilibrium. It can be concluded that the coating of a chip with a hydrophobic layer can be very beneficial to NLPF. Unlike the IMT chip, this parallel flow was stable for longer than a few seconds. As a comparison, all the OTS chip and Micronit chip values are given in one figure, figure (16). This figure shows two lines, each representing one chip. This representation makes comparing the chips more concise.

Figure (16) divides the pressure ratios of the regular Micronit chip and the OTS chip into flow pattern pieces. This is represented by the black lines. The Micronit flow pattern line shows four different flow patterns, of which two

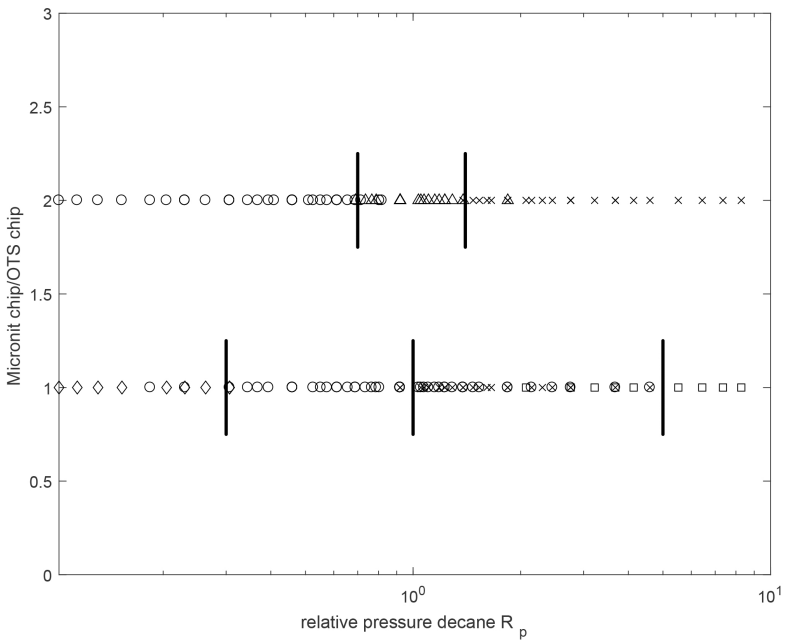

Figure 16: A plot of various flow ratio's between decane and water for an OTS coated Micronit chip and a regular Micronit chip. The relative flow ratios of the OTS chip are cross referenced with their original Micronit chip values. The top line represents the OTS chip, the bottom line represents the Micronit chip. The denotations for the flow patterns are similar to previous figures: $\diamond$ depicts organic droplet flow, $\circ$ depicts parallel flow with aqueous leakage, $\triangle$ depicts NLPF, $\times$ depicts parallel flwo with organic leakage, and depicts aqueous droplet flow.

droplet flow patterns. The OTS flow pattern line shows three, all parallel flow patterns. the coating eliminated any droplet flow in the Micronit chip. Stalling also was not present anymore. Finally, it enhanced the range in which NLPF could be found, which is between $0.7 < R_p < 1.3$.

However, after several days of measurements, the coating seemed to degrade. This was evident due to small air or aqueous phase pockets forming on the coated side of the channel. Since it is only a single layer modification of the channel, rapid degrading of the coating could be possible. This would mean this particular coating would be ineligible for the coating of microchannel in a radioactive process, since radiation will be able to break down the chemical bonds of the coating [28].

5 Conclusion

Viscous forces are the dominant factor in determining flow patterns in the IMT chip, if the interface stabilizes itself near the width $w^* = \frac{1}{2}w$, for Reynolds numbers in the order of $10^0 < Re < 10^1$ and for capillary numbers in the order of $10^{-4} < Ca < 10^{-3}$. However, the surface tension force and the inertial forces still impact the stability of the parallel flow in this regime negatively, since droplet flow formation was observed, and the interface was observed to be unstable.

The viscous forces are dependant on the velocity ratios and the viscosity ratios of the liquid phases. For high relative pressure, droplet flow patterns will be observed, while for relative pressure equaling unity, different parallel flow patterns are observed.

NLPF was established with the IMT chip. However, due to instability of the flow, caused by the surface tension and the inertial forces, but possibly also by the perturbation of the pumps, the NLPF only stabilized for short periods.

In the case of the Micronit chip, it was observed that the wettability of the channel was a major destabilizing factor for the flow patterns observed. NLPF was not found in this chip, due to inevitable parallel aqueous leakage. By selectively coating the chip with a hydrophobic layer, parallel flow was stabilized. This resulted in large, stable NLPF range. However, this particular coating will not be suitable for use in the extraction of radioactive materials, due to the possibility of rapid degrading when brought in contact with radiation.

A higher total viscous force at the outlet of the channel seems preferable for stability of parallel flow. This renders small variable changes negligible. Stall was observed in the Micronit channel, which could have been counteracted by higher viscous forces present.

6 Recommendation

In this paper, pressure differences at the outlet were deemed to be the dominant factor in determining flow patterns, due to viscous forces differences. However, pressure at the outlets was only changed by changing the flow rates of the pumps. Changing the pressure at the outlet due to varying height of the outlet tubing, length of the outlet tubing and outlet diameter could provide further insights for understanding parallel flow inside a microchannel.

The major factors that had negative influence on the parallel flow, were stability effects. Surface tension force, inertial forces and pump perturbation all caused instability in the interface. These effects are inherently coupled to two phase flow or experimental set-up. However, some effects have been proven to be successful in stabilizing the interface. Coating the chip selectively with a hydrophobic coating and installing a wave guide were measures to stabilize surface tension effects. An further examination of two phase interface stabilization could prove useful. This examination could examine coating effects further, by changing coating methods, coating surfaces and coating layers. A research could also specifically look at the effect of changing the cross-section of the tubing, including regular cross section changes, but also introducing the effects of wave guides.

7 Appendix

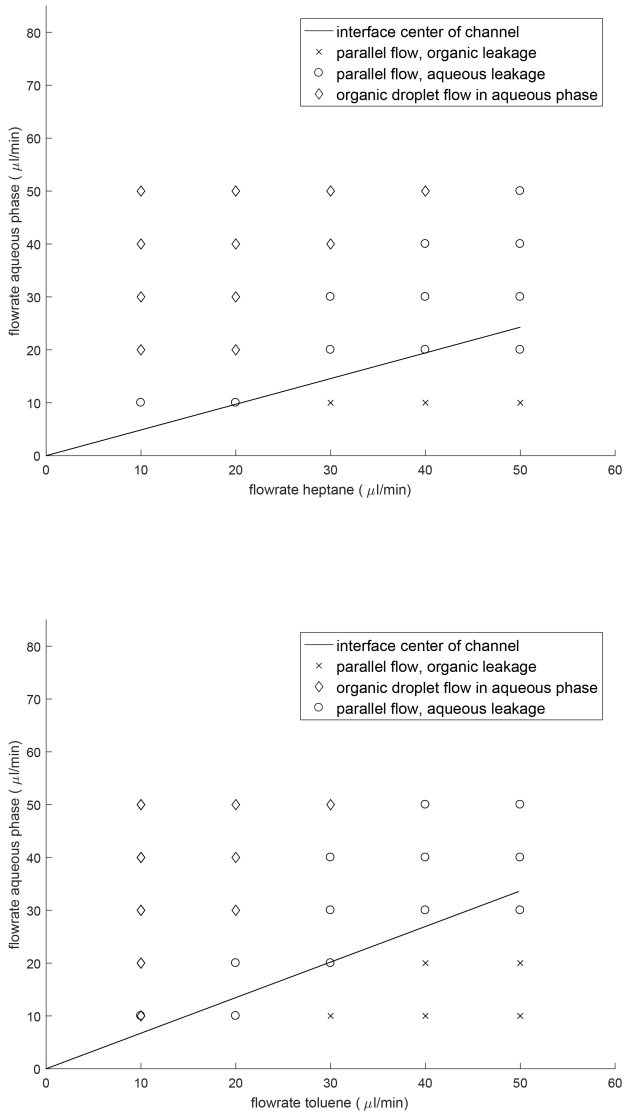

Figure 17: two flowchart plots, showing various ratio's between organic phases and water, together with a line that predicts where the interface should be in the middle of the channel for each respective organic phase.

References

[1] Burns JR, Ramshaw C. (2002) *A microreactor for the nitration of benzene and toluene.* Chemical Engineering Communications. 189, 1611–1628.

[2] Willaime H, Barbier V, Kloul L, Maine S, Tabeling P. (2006) *Arnold tongues in a microfluidic drop emitter.*

[3] Tokeshi M, Minagawa T, Uchiyama K, Hibara A, Sato K, Hisamoto H, Kitamori T. (2002) *Continuous-flow chemical processing on a microchip by combining microunit operations and a multiphase flow network.* Anal Chem. 74:1565–1571.

[4] Burns JR, Ramshaw C (2001) *The intensification of rapid reactions in multiphase systems using slug flow in capillaries.* Lab on a Chip. 1: 10-15

[5] Dummann G, Quittmann U, Groschel L, Agar DW, Worz O , Morgenschweis K. (2003) *The capillary-microreactor: a new reactor concept for the intensification of heat and mass transfer in liquid–liquid reactions.* Catalysis Today, 79: (1–4) 433–439.

[6] Pillai M.R.A. (2008) *Technetium-99m Radiopharmaceuticals: Manufacture of Kits* taken from official IAEA website

[7] Ciceri D, Perera JM, and Stevens G W. (2014) *The use of microfluidic devices in solvent extraction.* Journal of Chemical Technology and Biotechnology, 89(6):771–786

[8] Hibara A, Tokeshi M, Uchiyama K, Hisamot, H, Kitamori T. (2001) *Integrated multilayer flow system on a microchip.* Sci., 17: 89-93.

[9] Squires TM, Quake SR. (2005) *Microfluidics: Fluid physics at the nanoliter scale.* American Physical Society, 77(3):977-1026

[10] Bruus H. (2007) *Theoretical microfluidics*, chapters H1,2,5,11. Oxford University Press

[11] Blunt MJ. (2017) *Multiphase Flow in Permeable Media: A Pore-Scale Perspective* Cambridge University Press

[12] Young T. (1805). *An Essay on the Cohesion of Fluids.* Philosophical Transactions of the Royal Society A

[13] Richards TW, Carver EKJ. (1921) Journal of the American Chemical Society

[14] Aota A, Mawatari K, and Kitamori T. (2009) *Parallel multiphase microflows: fundamental physics, stabilization methods and applications.* Lab on a Chip, 9(17):2470–2476

[15] Kashid M, Kiwi-Minsker L. (2011) *Quantitative prediction of flow patterns in liquid–liquid flow in micro-capillaries.* Chemical Engineering and Processing: Process Intensification, 50(10):972-978

[16] Pohar A, Lakner M, Plazl I. (2012) *Parallel flow of immiscible liquids in a microreactor: modeling and experimental study.* Microfluidics and NanofluidicsJ, 12(1–4):307–316

[17] Zhao B, Moore J, Beebe S. (2001) *Surface-directed liquid flow inside microchannels.* Science 291(5506):1023-1026

[18] Zhao Y, Chen G, Yuan Q. (2006) *Liquid-Liquid Two-Phase Flow Patterns in a Rectangular Microchannel.* AlChe Journal, 52(12):4052–4060

[19] Tokeshi M. (2002) *Analytical Continuous-flow chemical processing on a microchip by combining microunit operations and a multiphase flow network.* Progress in Nuclear Energy, 47(1–4):434-438

[20] Sumner AL, Menke EJ, Dubowski Y, Newberg, YT Penner RM, Hemminger JC, Wingen LM, Brauers T, Finlayson-Pitts BJ. (2004) *The nature of water on surfaces of laboratory systems and implications for heterogeneous chemistry in the troposphere.* Physical Chemistry Chemical Physics, 6:604-613

[21] Glass NR, Tjeung R, Chan P, Yeo LY, Frienda JR. (2011) *Organosilane deposition for microfluidic applications* Biomicrofluidics,5(3):036501–036501-7.

[22] Ushikubo FY, BirribilliD FS, OliveiraR RB, Cunha L. (2014) *Y- and T-junction microfluidic devices: effect of fluids and interface properties and operating conditions.* Microfluidics and Nanofluidics, 17(4):711–720

[23] https://www.i-mt.co.jp/en/chip/

[24] Marmur A. (2003) *Wetting on Hydrophobic Rough Surfaces: To Be Heterogeneous or Not To Be?* Langmuir 2003, 19, 8343-8348

[25] Hirotada Hirama H, Wada S, Shimamura J, Komazaki Y, Inoue T, Torii T. (2017) *Surface modifcation of a glass microchannel for the formation of multiple emulsion droplets.* Microfluidics and Nanofluidics:21:91

[26] Zeppieri S, Rodríguez J, López de Ramos AL. (2001) *Interfacial Tension of Alkane + Water Systems* Journal of Chemical Engineering Data 46(5):1086–1088

[27] Saien J, Akbari S. (2006) *Interfacial Tension of Toluene + Water + Sodium Dodecyl Sulfate from (20 to 50) C and pH between 4 and 9.* Journal of Chemical Engineering Data, 51(5):1832–1835

[28] Wilski H. (1987) *The radiation induced degradation of polymers* International Journal of Radiation Applications and Instrumentation. Part C. Radiation Physics and Chemistry 29(1):1-14